Inorganica Chimica Acta 565 (2024) 121999

Contents lists available at ScienceDirect

Inorganica Chimica Acta

journal homepage: www.elsevier.com/locate/ica

Simultaneous hydroxido-, nitrato-, and phenoxido-bridged binuclear copper Schiff base complex for green catalytic click chemistry: Synthesis, structure, Hirshfeld surface analysis, theoretical study and photoluminescence spectra

Biplab Biswas [a,b], Bibhas Mondal [a], Partha Pratim Hajra [a], Corrado Rizzoli [c], Suman Mallick [d], Indrajit Saha [e], Swadhin Kumar Saha [a], Ujjal Kanti Roy [a,*], Rajat Saha [a,*]

[a] Department of Chemistry, Kazi Nazrul University, Asansol 713340, WB, India
[b] Department of Chemistry, Hooghly Mohsin College, Chinsurah 712101, WB, India
[c] Dipartimento SCVSA, Università di Parma, Parma 43124, Italy
[d] Department of Chemistry and Biochemistry, School of Basic Sciences & Research, Sharda University, Greater Noida 201310, UP, India
[e] Department of Chemistry, Ramakrishna Mission Residential College (Autonomous), Narendrapur 700103, WB, India

ARTICLE INFO

Keywords:
Binuclear copper (II) complex
Nitrate bridging
Hirshfeld surface analysis
Theoretical calculation
Catalytic CuAAC reaction

ABSTRACT

Catalytic click reactions are highly fascinating in chemical industries from several aspects like green synthesis, easy separation, nearly-perfect bond formation, etc. A new binuclear copper complex $[Cu_2(\mu\text{-}OH)(\mu\text{-}NO_3)(H_4L)(H_2O)(NO_3)]\cdot(H_2O)$ (where H_5L = 2,2′-((1E,1′E)-((2-hydroxy-5-methyl-1,3-phenylene)bis(methanylylidene))bis(azanylylidene))bis(propane-1,3-diol)) has been used for catalytic Huisgen 1,3-dipolar cycloaddition click reaction in water. The complex has been synthesized by using a multidentate compartmental ligand and characterized by single crystal X-ray crystallography along with spectral characterizations. The structural analysis shows that this binuclear complex crystallizes in the monoclinic space group $P2_1/c$ and both metal centers are bridged by a nitrate anion, a hydroxide ion, and a phenoxide group. Each discrete complex is connected by hydrogen bonding interactions to form a 3D supramolecular structure. Hirshfeld analysis and corresponding 2D fingerprint plots give a detailed information about the intermolecular interactions present in the complex. The complex also shows blue emission spectra. Density functional theory (DFT) and time dependent DFT (TDDFT) calculations have been carried out to rationalize the geometry and absorption spectrum of the complex. Afterward, the complex was used for the green catalytic click chemistry by optimizing the Huisgen 1,3-dipolar cycloaddition reaction. The complex shows high catalytic activity for copper catalyzed azide–alkyne cycloaddition (CuAAC) reaction in the aqueous phase with an average 80 % yield.

1. Introduction

The design of multinuclear metal complexes like bi-, tri-, and polynuclear transition metal-based complexes has gained much attention for their potential applications in various types of catalytic reactions [1–4]. To date, numerous molecular catalysts have been developed for the synthesis of a variety of organic molecules with diverse functional groups and different geometries. Triazoles are a class of *N*-heterocyclic organic molecules used in diverse applications from chemistry to material science to the medicinal industry [5–13]. A number of drug molecules with triazole scaffold have been developed as anticancer [14], antiviral [15], and anti-HIV agents [16,17]. Thus, there is a great interest in the synthesis of triazoles with high yield and low purification cost. In the past century, Huisgen and co-workers have developed a 1,3-dipolar cycloaddition reaction between azide and alkyne moieties to prepare triazoles [18]. However, this uncatalyzed thermal reaction proceeds at a slow rate and requires a temperature of 60–120 °C, which makes it vulnerable to the use of several azide precursors and also leads to a mixture of products [19].

Sharpless has introduced the term “click chemistry” as an efficient approach for the synthesis of diverse organic molecules following near-perfect carbon–heteroatom bond forming reactions by joining two

* Corresponding authors.
E-mail addresses: uroccu@gmail.com (U.K. Roy), rajatinorg1@gmail.com (R. Saha).

https://doi.org/10.1016/j.ica.2024.121999
Received 17 December 2023; Received in revised form 10 February 2024; Accepted 27 February 2024
Available online 29 February 2024

molecular fragments [20]. Such click reactions proceed under mild conditions with quantitative yields and high regioselectivity [21]. In 2002, two different research groups namely Medlals et al., [22] and Sharpless et al., [23] have reported the copper(I) catalyzed Huisgen [3+2] cycloaddition reaction to synthesize 1,4-disubstituted 1,2,3-triazoles in very high yields with few or no side products. Followed by, a new research theme on copper-catalyzed azide–alkyne [3+2] cycloaddition (CuAAC) has become a leading method in organic chemistry for the synthesis of large molecules by using 1,2,3-triazole as a bridging block unit [24–30]. Since then, a number of research groups have used other metal ions such as silver [31], ruthenium [32], iridium [33], and zinc [34], for the catalytic azide–alkyne cycloaddition (AAC) reactions.

Copper (I) species are thermodynamically unstable and thus any other copper source that can produce catalytically active Cu(I) species, e.g. Cu(II) salts or their complexes, metallic copper, copper-nanoparticles, etc., has been used as a catalyst in the CuAAC reaction [35]. However, the Sharpless–Fokin catalyst composed by the combination of $CuSO_4{\cdot}5H_2O$ and sodium ascorbate in water has been considered as the most effective one, *in-situ* reduction of Cu(II) by sodium ascorbate produces the catalytically active copper (I) species [36]. The main drawback of this method is the instability of organic azides and the corresponding potential risk of explosion. To overcome this limitation, researchers have attempted to synthesize organic azides by *in situ* reaction between organic halides or aryl boronic acids with sodium azide [37–42]. However, the removal of the catalyst from the reaction mixture is another big challenge due to its toxicity, which causes serious concern over its uses in the synthesis of bio-molecules [43]. In this regard, major focus has been given to the use of catalysts where the catalysts remain dissolved in water and the organic precursors as well as the products are in the solid state [44–47]. Moreover, the use of water as a green solvent allows an easier purification of the products, and *in situ* generated organic azides are immediately consumed in the next step of the reaction [48–51]. Several research groups have used different copper(II) complexes for the said CuAAC reaction in aqueous medium [52,53]. In some cases, metal-azide complexes, inspite of using NaN_3, are also used as the catalyst and the synthesized triazole has been found to bind with the metal centers [54,55]. The complexes are also used as a heterogeneous catalysts by supporting them on different solid substrates like silica, SBA-15, etc [56,57]. In several cases, the authors have reported that these copper (II) complexes show low conversion (~25–50 %) at room temperature [58] though it is dependent on the amount of catalyst used. With the above consideration in mind, we report herein the synthesis, and characterization of a water-soluble binuclear copper (II) complex and its application in the catalytic click CuAAC reaction. Our complex shows a moderate yield (60 % with 3 mol % of catalyst) at room temperature in aqueous medium.

2. Experimental section

2.1. Materials and methods

The used AR grade solvent methanol was of Spectrochem. The 1,3-diamino-2-propanol (serinol) utilized was purchased from commercial sources of Aldrich. Emplura grade copper(II) nitrate trihydrate was bought from Merck (India). All the reagents acquired were used without further purification. 2-hydroxy-5-methylisophthalaldehyde was synthesized by following the procedure described in the literature [59]. The elemental analysis (C, H, N) data were collected using a PerkinElmer 240C elemental analyzer. The Nicolet Impact 410 spectrometer was utilized to acquire Fourier transform infrared (FT-IR) data by using KBr pellets in the range of 400–4000 cm^{-1}. Absorption and emission spectra were recorded on a SHIMADZU UV 1800 and a Perkin Elmer LS −55B fluorescence spectrophotometer instrument, respectively, in the solution phase. ^1H NMR spectra were recorded on a 400 MHz Bruker NMR spectrometers using TMS as the internal standard. Chemical shifts are reported in parts per million (ppm). When peak multiplicities are given, the following abbreviations are used: s, singlet; br s, broad singlet; d, doublet; t, triplet; m, multiplet.

2.2. Synthesis of complex $[(C_{15}H_{21}N_2O_5)Cu_2(\mu_2\text{-}OH)(\mu_2\text{-}NO_3)(H_2O)\cdot NO_3].H_2O$

The H_5L ligand has been synthesized by reacting 2-hydroxy-5-methylisophthalaldehyde with 2-amino-1,3-propanediol in 1:2 ratio in methanol under heating (~50 °C) condition. The purified ligand was characterized by CHN, IR and NMR study and the detailed synthesis is given in the supporting information file. 1 mmol of the ligand H_5L was dissolved in 10 ml methanol to which a methanolic solution (5 ml) of 3 mmol $Cu(NO_3)_2{\cdot}3H_2O$ was poured with continuous stirring to obtain a greenish blue solution. The reaction mixture was stirred for 4 h more. The solution thus obtained was filtered and kept for crystallization. Blue rod-shaped crystals were obtained after 2 days. Yield: 85 % (w.r.t. ligand). Anal. Calc. for formula: C, 29.34; H, 4.27; N, 9.13. Found: C, 29.33; H, 4.29; N, 9.12. ICP-MS: Cu, 20.71, Found: Cu, 20.75. Important IR peaks (KBr, cm^{-1}) are: 3332, 1627, 1317.

2.3. Single crystal data collection and structure refinement

Suitable single crystal of the complex was mounted on a Bruker APEX II diffractometer equipped with a graphite monochromator and Mo-K_α (λ = 0.71073 Å) radiation. Unit cell parameters were determined by using the APEX2 [60] program. Data reduction was carried out by the SAINT [60] program and correction for absorption was performed using the SADABS [60] program. The structure was solved by direct methods using SHELXS-2018/3 [61] embedded in the WINGX software package [62] and refined using SHELXL-2019/3 [63]. Subsequent difference Fourier synthesis and least-square refinement revealed the positions of the remaining non hydrogen atoms. Non-hydrogen atoms were refined with independent anisotropic displacement parameters. The hydroxyl H atoms could be located in a difference Fourier map and were refined as riding $U_{iso}(H) = 1.5\ U_{eq}(O)$. The water H atoms could also be located in a difference Fourier map and refined by constraining the O—H distance to be 0.82(1) Å and the H…H separation 1.296(2) Å, with $U_{iso}(H) = 1.5\ U_{eq}(O)$. All other H atoms were placed geometrically and refined using a riding atom approximation, with C—H = 0.93–0.98 Å, and with $U_{iso}(H) = 1.2\ U_{eq}(C)$ or $1.5\ U_{eq}(C)$ for methyl H atoms. A rotating model was used for the methyl and hydroxyl groups. One outlier (200) was omitted in the last cycles of refinement. All Figures were drawn by using PLATON [64] and ORTEP [65]. Data collection and structure refinement parameters and crystallographic data for **complex** are given in Table 1.

2.4. Hirshfeld surface analysis

The nature of the noncovalent interactions present within a crystal system can be visually depicted and quantified through Hirshfeld surface analysis. Hirshfeld surface (HS) as constructed from electron distribution analysis around a molecule visualizes intermolecular interactions in molecular crystals. The two-dimensional (2D) fingerprint plots are acquired from the HS analysis and can identify each type of intermolecular interaction within supramolecular and coordination compounds and their relative contributions can be obtained from the area of the surface. For each point on HS d_i is the well-defined distance from the nearest nucleus internal to the surface and analogously, d_e is the distance from the nearest nucleus external to the surface. The normalized contact distance can be defined by

$$d_{norm} = \frac{(d_i - r_i^{vdW})}{r_i^{vdW}} + \frac{(d_e - r_e^{vdW})}{r_e^{vdW}},$$

where r_i^{vdW} and r_e^{vdW} are the van der Waals radii of the appropriate atoms internal and external to the HS. Hirshfeld surfaces and their corresponding 2D fingerprint plots were calculated over the constituent ionic

Table 1
Crystallographic data collection and refinement parameters of **complex.**

CCDC	2310372
Formula	$C_{15}H_{26}Cu_2N_4O_{14}$
Formula weight	613.48
Crystal system	Monoclinic
Space group	$P2_1/c$
a (Å)	9.894(2)
b (Å)	27.884(6)
c (Å)	8.561(2)
α (°)	90
β (°)	95.898(4)
γ (°)	90
V (Å^3)	2349.3(9)
Z	4
ρ_{calc} (g/cm^3)	1.735
μ (Mo Kα) (mm)	1.887
F(000)	1256
crystal size (mm^3)	0.14 × 0.15 × 0.28
Temperature, T (K)	294
$\theta_{min\text{-}max}$ (°)	1.5, 25.5
Total data	25,919
Unique data	4363
R_{int}	0.040
Observed data [I > 2.0 σ(I)]	3761
N_{ref}	4363
N_{par}	334
R	0.0389
wR_2	0.1190
S	1.07

and molecular geometries using CRYSTALEXPLORER 17.5 software package [66,67]. The properties like normalized contact distance d_{norm}, shape index, curvedness, and fragment patch were mapped over the Hirshfeld surface and plotted with the appropriate color scale. The 2D fingerprint plots were presented as d_e vs d_i.

2.5. Computational methods

The ORCA 3.1 software packages were used for DFT computations [68]. The geometry of the cationic complex was optimized in the gas phase ($S = 1$) using the Cartesian coordinates of the crystal structure and employing the Becke–Perdew (BP86) functional [69,70] and RI/J approximation [71]. Geometry optimization was converged with the def2-SV(P) basis set [72] and def2-SVP/J auxiliary basis set [73,74] for C and H atoms, def2-TZVP(−f) basis set [75] and def2-TZVP/J auxiliary basis set [68] for N, and O atoms and def2-TZVPP basis set [69,70] and def2-TZVPP/J auxiliary basis set [68] for Cu atoms including the ZORA (zeroth-order regular approximation) [76]. Electronic transition energies and intensities were computed using the time-dependent DFT (TDDFT) method within the Tamm–Dancoff approximation [77]. These calculations employed the B3LYP functional [72] and COSMO methodology [78] using $\varepsilon = 32.7$ for the CH_3OH solvent. Forty excited states were calculated by including all one-electron excitations within an energy window of ±3 Hartree with respect to the HOMO/LUMO energies. Isosurface plots of molecular orbitals were generated using the gOpenMol 3.00 program [79,80] with isodensity values of 0.04.

2.6. Catalytic experimental details

Allyl bromide (4 mmol), sodium azide (4 mmol), and the catalyst (5 mmol%) were added to water and stirred for 1 h at room temperature in a round bottom flask. In the next step, phenylacetylene (4 mmol) was put into the reaction mixture and stirring was continued until complete consumption of phenylacetylene. The progress of the reaction was screened through TLC monitoring (hexane: ethyl acetate = 9:1). After completion, the reaction mixture was extracted with ethyl acetate thrice. The combined organic layer was dried over Na_2SO_4, filtered, and concentrated under vacuum to afford the crude product. The solid crude product was then purified by column chromatography (silica 100–200 mesh, ethyl acetate-hexane 5–10 %) to afford the desired triazole product.

3. Result and discussion

3.1. Synthesis and characterization

Utilization of phenolic-OH containing compartmental ligands has been successfully employed to design multinuclear metal complexes [81,82]. The goal of such utilization goes with the fact that more than one metal center will bind in the different compartments of the ligand as well as the phenoxido group will act as a bridge between metal centers. In this attempt, we have synthesized the complex in two steps (Scheme 1). In the first step, we have synthesized and characterized the ligand. The Schiff base condensation reaction between the dialdehyde and the serinol in the 1:2 ratio leads to the formation of the ligand H_5L. IR spectroscopic analysis clearly demonstrates the formation of the ligand (Fig. S1). The peak at 1644 cm^{-1} in the infrared spectrum of the ligand surfaces is due to the presence of the azomethine (C═N) group [83]. The synthesized ligand is further used for metal complex formation. During the synthesis, only the phenolic-OH group gets deprotonated but not the alcoholic –OH groups and the ligand acts as H_4L^- anion. The appearance of the sharp peak for the azomethine group within the IR spectrum of the complex (Fig. S4) at a lower frequency, 1627 cm^{-1}, is indicative of its involvement in coordination with the metal center [83]. The broad band centered at 3332 cm^{-1} in the complex, presumably, is the result of the overlapping of the bands for μ_2-bridged O—H, O—H of coordinated water, coordinated and uncoordinated alcoholic O—H groups of the Schiff base. The sharp peak at 1317 cm^{-1} which is absent in the ligand may arise due to the coordinated nitrate anions. The sharpness of the peak indicates the coordinated nature of the nitrate ions. The overall charge of the binuclear complex is compensated by the coordination of two nitrate anions and one hydroxide ion formed from water dissociation.

3.2. Molecular and supramolecular structure of the complex

From the SC-XRD data, it is seen that the complex crystallizes in the monoclinic space group $P2_1/c$. The asymmetric unit consists of one pentadentate H_4L^- ligand, one μ_2- bridged NO_3^- anion, one monodentate NO_3^- anion, one μ_2-OH^- ion, one coordinated water molecule, two copper (II) ions, and one water molecule of crystallization (Fig. S5). Both the metal centers are coordinatively saturated and show a six-coordinated distorted octahedral geometry. For the Cu1 center, the coordination geometry is fulfilled by the *mer*-arranged O1, O3 and N1 atoms of H_4L^-, one oxygen atom (O8) from the μ_2-bridged nitrate anion, one oxygen atom (O10) from the monodentate nitrate anion, and the μ_2-OH^- anion (O2). The best equatorial plane (r.m.s. = 0.0122 Å) is provided by the O1/O2/O3/N1 set of atoms, with the metal displaced by only 0.0081(4) toward O10. The angle formed by the O8…O10 line through the apical nitrate oxygen atoms and the normal to the equatorial plane is 0.98 (19)°. For the Cu2 center, the octahedral environment is provided by the *mer*-arranged O1, O5, and N2 atoms of ligand H_4L^-, one oxygen atom (O7) from the μ_2-bridged nitrate anion, one coordinated water oxygen atom (O13), and the μ_2-OH^- anion (O2). The coordination geometry resembles that observed for Cu1, with the best equatorial plane defined by the O1/O2/O5/N2 donor atoms (r.m.s. = 0.0387 Å; the metal lies almost exactly on the mean plane, being displaced by 0.0001(4) Å toward O7) and the O7…O13 line through the apical atoms forming an angle of 2.18(9)° with the normal to the equatorial plane. The six-membered chelation rings are almost planar (puckering parameters: $Q = 0.079(2)$ Å, $\theta = 129(2)°$, $\varphi = 133(2)°$ and $Q = 0.075(3)$ Å, $\theta = 106(2)°$, $\varphi = -98(2)°$ for Cu1/O1/C1/C2/C7/N1 and Cu2/O1/C1/C6/C11/N2 respectively), while the five-membered chelation rings adopt an envelope conformation (puckering parameters: $Q = 0.377(4)$ Å, $\varphi = -104.8(4)°$ and $Q = 0.365(3)$ Å, $\varphi = -105.7(4)°$ for Cu1/O3/C9/C8/N1

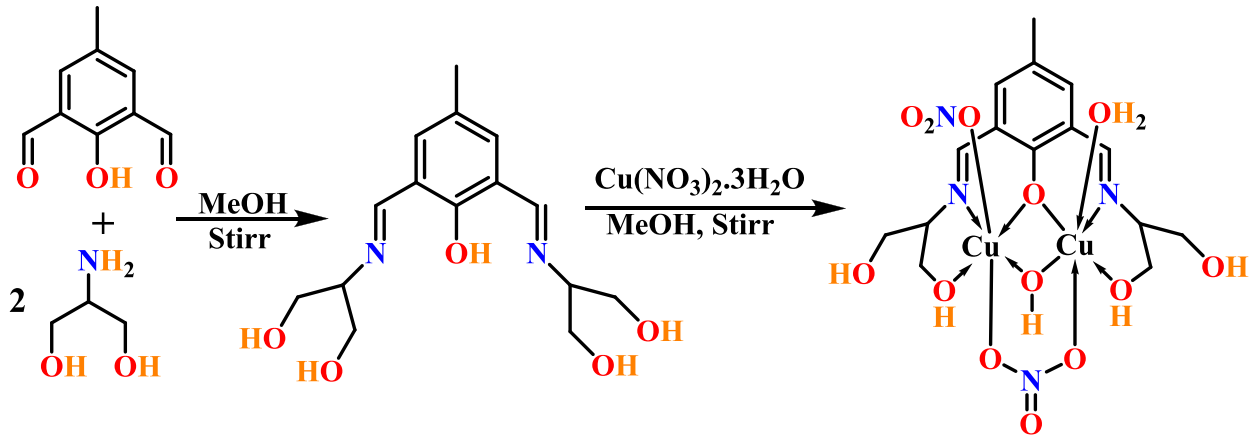

Scheme 1. Synthesis of complex.

and Cu2/O5/C13/C12/N2, respectively) with atoms C9 and C13 as flaps. The coordination mode of the ligand prevents the O4 and O6 hydroxy groups from binding with the metal center. The Cu-N bond distances are in the range of 1.929(3) Å and 1.933(3) Å while the Cu-O bond distances vary between 1.920(2) Å and 2.627(3) Å. The bond distances Cu1-O10, Cu1-O8, Cu2-O7, and Cu2-O13 are respectively 2.627(3) Å, 2.450(3) Å, 2.536(3) Å, and 2.504(3) Å and found to be much larger than the other Cu-O bond distances i.e., the axial elongation of Cu-O bond is observed which might be attributed to the Jahn-Teller distortion inherent in a Cu(II) d^9 system [81,84,85,86]. The Cu1···Cu2 separation within the complex is 2.8880(8) Å and is longer than the the sum of the van der Waals radii (2.56) Å. Selected coordination bond lengths and bond angles are presented in Table S1.

Each discrete binuclear complex is connected by intermolecular hydrogen bonds (O3-H3O···O6 and O6-H6O···O10 along the ***a***-axis; O5-H5O···O2 and O4-H4O···O11/O12 along the ***b***-axis and O13-H132···O8/O9 along the ***c***-axis) to form a 3D metal–organic supramolecular host (MOSH) structure (Fig. 1). This supramolecular host structure contains discrete supramolecular pockets to accommodate guest water molecules (Figs. 2a and S7). Two water molecules are present within each supramolecular pocket through hydrogen bonding interactions with the hydroxide groups (O2-H2O···O14), coordinated water molecules (O14-

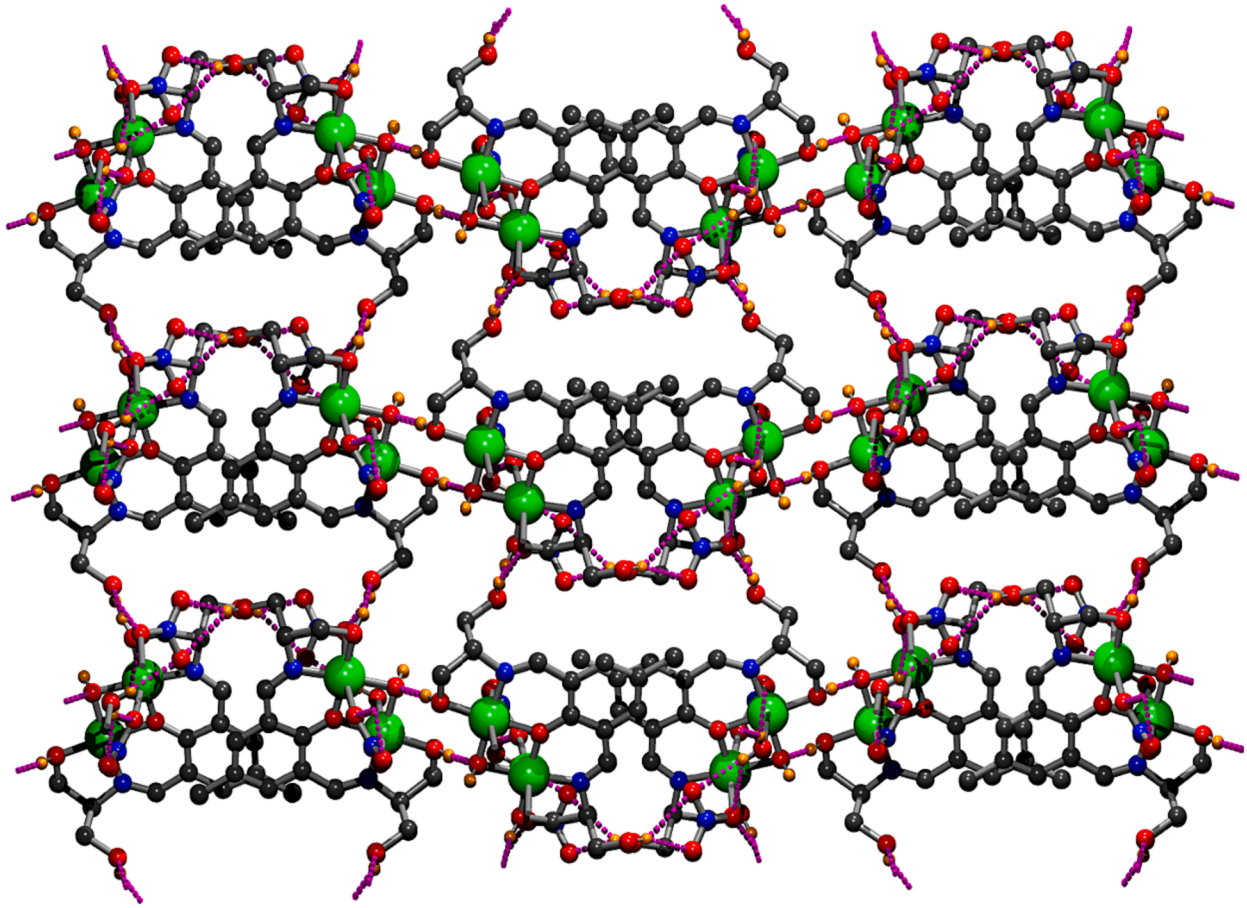

Fig. 1. 3D supramolecular structure of the complex formed by hydrogen bonding interactions between each metal–organic complex. (C: Grey, H: Orange, N: Blue, O: Red, Cu: Green, Hydrogen bond: Magenta).

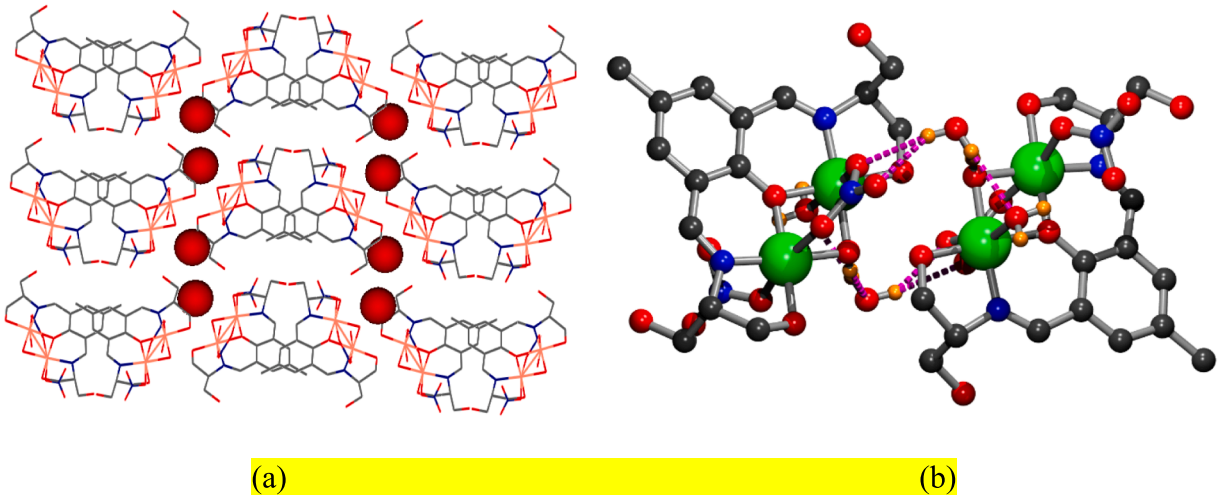

Fig. 2. Guest water molecules are present within the pockets (a) through hydrogen bonding interactions (b) (C: Grey, H: Orange, N: Blue, O: Red, Cu: Green, Hydrogen bond: Magenta).

H141···O13), and nitrate groups (O14-H142···O9 and O14-H142···O7) (Fig. 2b). The crystal structure is further stabilized by non-classical intermolecular C—H···O hydrogen bonds. All the hydrogen bond dimensions are presented in Table S2.

A CCDC search shows that there are only eight examples of binuclear copper complexes with simultaneous phenoxido-, hydroxido-, and nitrato- bridging [81,82,86,87]. The complex formation proceeds with the binding of the two different metal centers through phenoxido bridges. Subsequently, the other donor centers of the ligand coordinate with the metal centers to further stabilize the binuclear complex.

3.3. Hirshfeld surface analysis

Hirshfeld surface analysis has been carried out over the complex to gain an insight on the intermolecular interactions present within the overall 3D supramolecular structure and the guest water molecule. Different research groups have analysed the supramolecular interactions present in coordination complexes through Hirshfeld surface analysis [88–90]. Fig. S8 depicts the d_{norm} surface mapped over the complex showing intense red spots close to the four hydroxide groups and oxygen atoms of nitrate groups. The 2D fingerprint plot (Fig. S9) supports the presence of O···H interactions between hydroxide oxygen atoms and hydrogen atoms of water molecules and neighboring nitrate groups as the predominant interaction (26.4 %). Also, O···H/H···O hydrogen bonding interactions show sharp spikes at ($di = 0.95$, $de = 0.60$ Å) and at ($di = 0.60$ Å, $de = 0.95$ Å). An additional contribution to the HS comes from the H—H (36.3 %), C—H (3.8 %), and N—H (1.1 %) interactions.

3.4. Absorption and emission spectra of the complex

Both the absorption and emission spectra were measured in methanolic solution. The complex shows absorption maxima at 373 nm with a shoulder at 447 nm and another peak with low intensity at 630 nm (Fig. S10). The low-intensity band at 630 nm appears for d-d transition. The peak at 373 nm arises due to mainly intra-ligand charge transfer (ILCT). A small shoulder at 447 nm appears to overlap with the intense ILCT. This transition may be ascribed to a d-d transition in pseudo-octahedral geometry. Solution phase luminescence spectra of the complex show weak emission at 420 nm upon excitation at 373 nm (Fig. S11).

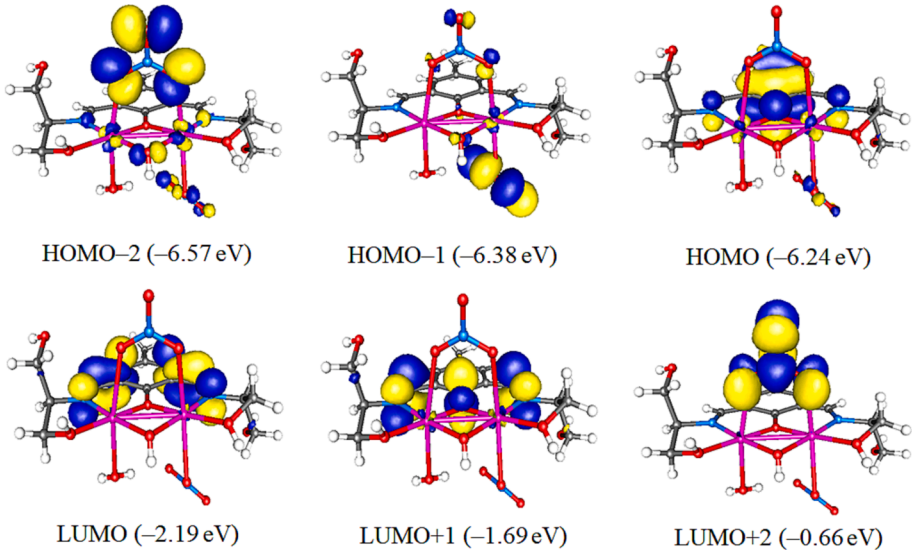

Fig. 3. Spin-up frontier molecular orbitals (isodensity value ± 0.04) of the complex, showing the orbital energies. The outer water molecule has not been taken for computation.

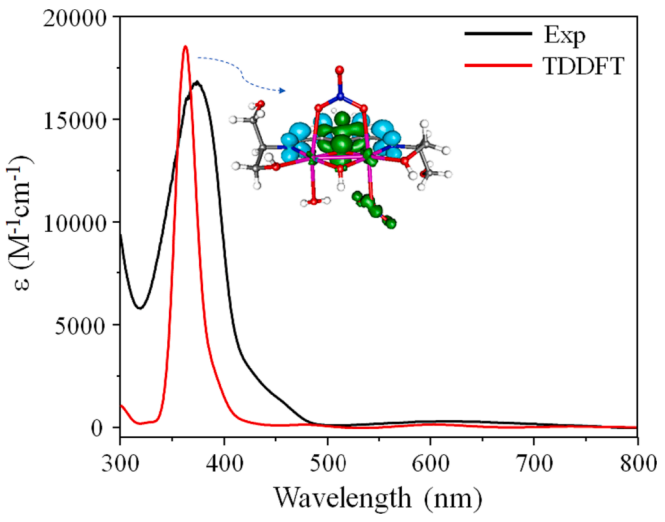

Fig. 4. Comparison between experimental and TDDFT-calculated absorption spectra for the cationic complex. The absorption bands are assigned on the basis of the corresponding electron density difference map (EDDM) where electron gain is denoted by cyan color and electron loss by green color.

3.5. Density functional theory (DFT) calculations

To get the nature of the frontier molecular orbitals (FMOs), the single point energy computation at the DFT level was performed on the energy-optimized geometry of the complex. The isodensity plots of the spin-up (α) FMOs together with the orbital energies are shown in Fig. 3. The HOMO is mainly composed of the π orbitals of the H_5L ligand, while HOMO–1 and HOMO–2 are the π orbital of nitrate ligands. The LUMO and LUMO + 1 consist π* orbitals of the H_5L ligand. The HOMO–LUMO gap for the complex is 4.05 eV.

The absorption spectrum of the complex was further scrutinized by time-dependent DFT (TDDFT) calculation. The corresponding simulated UV–vis absorption spectrum in comparison with the experimental spectrum is shown in Fig. 4. The complex displays an absorption band near 373 nm which corresponds to the calculated absorption at 364 nm (3.406 eV, $f = 0.125881977$). This spectral feature is mainly due to the H (α) → L (α) and H (β) → L + 2 (β) transitions. The electron density difference map (EDDM) for this electronic transition clearly indicates the ILCT nature of the band (Fig. 4). Therefore, the computational studies explain well the absorption spectrum of the complex.

3.6. Catalytic click chemistry

Finally, we have successfully used the complex as catalyst in the [3+2] cycloaddition of terminal alkynes and organic azides in catalytic CuAAC click reactions. All the reactions were performed in a one mmol scale relative to alkyne and azide reagents in 2 ml of solvent at room temperature in N_2 atmosphere. In the present study, the reduction of Cu (II) Schiff base complex does not require any further additive and thus we have done without using any other additive like sodium ascorbate [91]. In recent years several catalytic systems based on Cu(II) complexes for the click synthesis of triazoles have also been reported where the catalyst does not require any reducing agent [54,92,93]. Bikas et al., have performed significant research using copper(II) complexes under both homogeneous and heterogeneous conditions [54,56,94]. As a medium, water was used due to its benign nature for this multicomponent click reactions as the catalyst is readily soluble in water.

To optimize the proper synthetic condition and standardization, we chose allyl bromide, NaN_3, and phenylacetylene as reacting components for the CuAAC reaction. The initial reaction was carried out using 4 mmol of each reactant: allyl bromide, sodium azide and phenylacetylene in presence of the complex (5 mol%) as catalyst (Table 2). Allyl bromide, sodium azide (4 mmol), and the catalyst were added to water and stirred for 1 h at room temperature to form organic azide. In the next step, phenylacetylene was added to the reaction mixture and stirred until complete consumption of phenylacetylene and monitored by TLC (hexane: ethyl acetate = 9:1 *v/v*). The solid crude product was isolated and purified by column chromatography. The overall yield of the desired product is 72 % (entry 2). A similar reaction was carried out without using complex and it shows no product formation even after a long reaction time (entry 1). We have also observed that the product conversion is also dependent on the catalyst amount used in the reaction – by decreasing the catalyst amount to 3 mol% the overall yield also reduced to 60 % (entry 3) but further increasing more than 5 mol% has no significant impact on the yield of the reaction (entry 4). Later we have attempted to monitor the reaction temperature. As the reaction temperature increases to 90 °C, less time is required for 80 % conversion (entry 5). We have also studied the solvent screening for this catalytic CuAAC reaction and this reveals that organic solvents like tetrahydrofuran, dichloroethane, acetonitrile, dioxane, ethanol, toluene, acetone, etc. were found to be less effective giving similar or lower yield (entries 6–12) compared to that in water. So, water is the choice of solvent (entry

Table 2
The results for different conditions on the azide-alkyne cycloaddition.

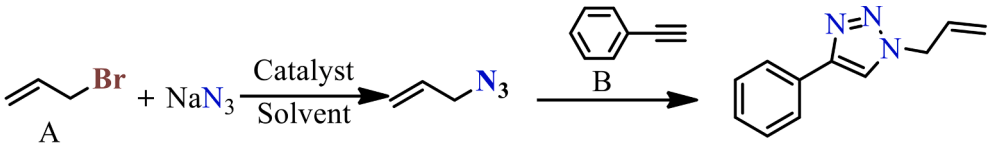

Entry	Catalyst Loading (mol %)	Solvent	Temp (°C)	Time (h)	Yield (%)
1	–	H_2O	r.t.	12	–
2	5	H_2O	r.t.	1 + 7	72
3	3	H_2O	r.t.	1 + 7	60
4	7	H_2O	r.t.	1 + 7	72
5	5	H_2O	90	1 + 4	80
6	5	C_2H_5OH	90	1 + 4	55
7	5	CH_3CN	90	1 + 4	50
8	5	Toluene	90	1 + 4	52
9	5	Acetone	70	1 + 4	58
10	5	DCE	50	1 + 4	53
11	5	THF	80	1 + 4	58
12	5	Dioxane	90	1 + 4	50

Conditions: Halide (A) 4 mmol, NaN_3 4 mmol, Solvent 4 ml, Phenylacetylene (B) 4 mmol.

Table 3
Substrate scope of catalytic Azide-Alkyne Cycloaddition (AAC).

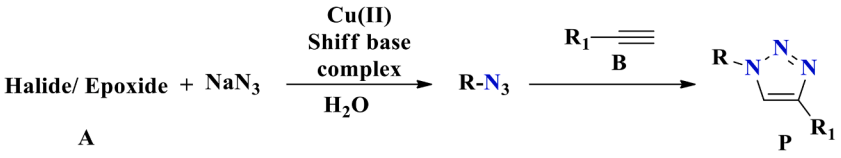

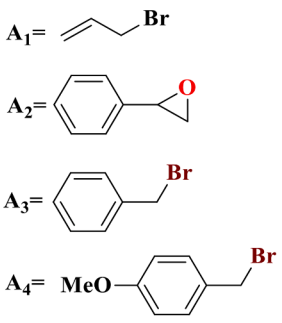

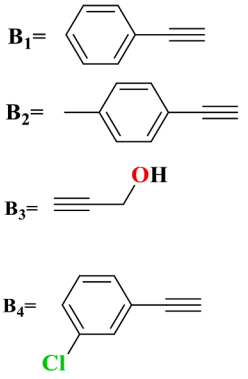

≠	Component A	Component B	Product	Time (h)	Yield (%)
1	A_1	B_1	P_1 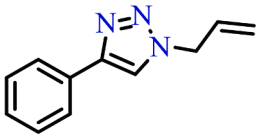	1 + 4	80
2	A_2	B_2	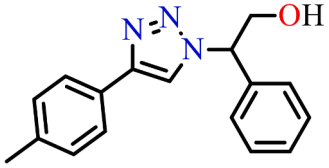 P_2	1 + 4	85
3	A_3	B_1	P_3 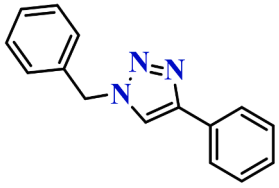	1 + 4	89
4	A_4	B_3	P_4 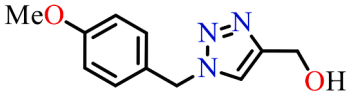	1 + 4	76
5	A_2	B_4	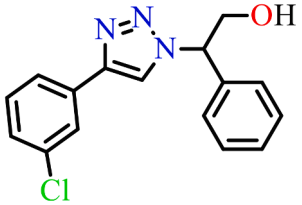	1 + 5	83

Conditions: Epoxide/Halide 4 mmol, NaN_3 4 mmol, solvent 4 ml H_2O, acetylene 4 mmol, 90 °C, catalyst 0.2 mmol.

5) for this reaction considering its green nature. The long time for conversion observed in water is presumably due to the lack of solubility of the organic substrates and products in this medium, whereas the catalyst is soluble. In the reaction, the substrates are not properly soluble (dispersed) in water which is in agreement with similar previous observations [94–96]. Based on these results, it appeared that the best yield to catalyst compromise is provided in entry 5 and we have followed this optimized condition to carry out further reactions with different substrates.

Water-like eco-benign solvents and one-pot multi-component single-step reactions are vital and important issues from a green chemistry prospect. For the smooth reaction, the starting material need not be completely soluble and the filtration of the end product from the solution may be the only purification step in many cases. With this background, the present click catalysis is a smart choice. Moreover, the complex is not air and moisture sensitive. In aqueous conditions, they can also produce the desired products selectively in good to excellent yields and the reaction time is relatively short (Table 3). Now, we have performed the reaction by using styrene oxide and substituted and unsubstituted benzyl bromide etc in place of allyl bromide in the optimized reaction conditions (Table 3). Substituted phenylacetylene, propargyl alcohol, and their derivatives can replace phenylacetylene successfully in the present reaction conditions. We have successfully applied the Schiff Base complex for the CuAAC reaction to synthesize 1,4 disubstituted-1,2,3-triazoles in excellent yield under an aqueous environment.

4. Conclusion

In summary, we have presented the catalytic CuAAC click reaction by a binuclear copper complex. The complex has been synthesized by using a compartmental ligand and a complex core is formed by simultaneous nitrato-, phenoxido-, and hydroxido- bridging. The supramolecular host structure formed by hydrogen bonding interactions among the binuclear metal–organic complexes is able to accommodate one guest water molecule. Hirshfeld surface analysis and corresponding 2D fingerprint plots clearly demonstrate the presence of hydrogen bonding interaction as the most significant weak interaction for the supramolecular host structure formation. The theoretical study presents the excellent matching between the experimental spectral results. This water soluble and blue luminescent complex has been used for the catalytic CuAAC click reaction and it shows excellent catalytic efficiency in the aqueous phase.

CRediT authorship contribution statement

Biplab Biswas: Writing – review & editing, Writing – original draft, Investigation, Conceptualization. **Bibhas Mondal:** Writing – original draft, Investigation, Data curation, Conceptualization. **Partha Pratim Hajra:** Data curation. **Corrado Rizzoli:** Writing – review & editing, Writing – original draft, Investigation, Formal analysis, Data curation. **Suman Mallick:** Writing – review & editing, Writing – original draft, Investigation, Conceptualization. **Indrajit Saha:** Writing – original draft, Resources, Data curation, Conceptualization. **Swadhin Kumar Saha:** Writing – original draft, Validation, Investigation. **Ujjal Kanti Roy:** Writing – review & editing, Writing – original draft, Validation, Supervision, Investigation, Data curation, Conceptualization. **Rajat Saha:** Writing – review & editing, Writing – original draft, Visualization, Validation, Supervision, Project administration, Investigation, Conceptualization.

Declaration of competing interest

The authors declare that they have no known competing financial interests or personal relationships that could have appeared to influence the work reported in this paper.

Data availability

No data was used for the research described in the article.

Acknowledgements

This work was supported by funding from TARE, SERB to R.S. (TAR/2018/000744). R.S. also acknowledges UGC for their STIDE GRANT to Kazi Nazrul University (Ref No: KNU/R/Letter/913/21). I.S. thanks SERB (EEQ/2019/000372 to I.S) for financial assistance. S.M acknowledges the support of Computational Chemistry Lab (CCL) of the Department of Chemistry & Biochemistry at Sharda University.

Author Contributions

RS and BB have designed the complete research work. BM, PPH and UKR have performed the catalysis experiment. CR has done the crystallographic analysis. SM has performed the theoretical calculations. SKS has done the Hirshfeld surface analysis. IS has done all the optical measurements. All authors have jointly written the manuscript.

Appendix A. Supplementary data

CCDC 2310372 contains the supplementary crystallographic data for the complex. These data can be obtained free of charge from The Cambridge Crystallographic Data Centre via www.ccdc.cam.ac.uk/data_request/cif. Synthesis of the ligand, table of bond distances and angles, hydrogen bond dimensions, IR, absorption spectra, NMR spectra, ORTEP diagram, supramolecular structures, emission spectra, theoretical optimized geometries, etc. are given in the supporting information file. Supplementary data to this article can be found online at https://doi.org/10.1016/j.ica.2024.121999.

References

[1] K.C. Gupta, A.K. Sutar, Coord. Chem. Rev. 252 (2008) 1420–1450.
[2] K.D. Vogiatzis, M.V. Polynski, J.K. Kirkland, J. Townsend, A. Hashemi, C. Liu, E. A. Pidko, Chem. Rev. 119 (2019) 2453–2523.
[3] F. Franco, C. Rettenmaier, H.S. Jeon, B.R. Cuenya, Chem. Soc. Rev. 49 (2020) 6884–6946.
[4] F. Glaser, O.S. Wenger, Coord. Chem. Rev. 405 (2020) 213129.
[5] Q. Deng, N. N. Ding, X. L. Wei, L. Cai, X. P. He, Y. T. Long, G. R. Chen, K. Chen, *Corr. Sci.* 64 (2012) 64–73.
[6] W. Dehaen, V. A. Bakulev, Springer International Publishing, 2015, Switzerland.
[7] C. Ye, G.L. Gard, R.W. Winter, R.G. Syvret, B. Twamley, J.N. Shreeve, Org. Lett. 9 (2007) 3841–3844.
[8] E. Bonandi, M.S. Christodoulou, G. Fumagalli, D. Perdicchia, G. Rastelli, D. Passarella, Drug Discov. Today 22 (2017) 1572–1581.
[9] N.G. Aher, V.S. Pore, N.N. Mishra, A. Kumar, P.K. Shukla, A. Sharma, M.K. Bhat, Bioorg. Med. Chem. Lett. 19 (2009) 759–763.
[10] M.R.E.S. Aly, H.A. Saad, M.A.M. Mohamed, M.A.M. Bioorg, Med. Chem. Lett. 25 (2015) 2824–2830.
[11] R. Kharb, M. S. Yar, P. C. Sharma, Curr. Med. Chem. 18 (2011) 3265–3297.
[12] [12] N. W. Smith, A. Alonso, C. M. Brown, S. V. Dzyuba, Biochem. Biophys. Res. Commun. 391 (2010) 1455–1458.
[13] Y.H. Lau, P.J. Rutledge, M. Watkinson, M.H. Todd, Chem. Soc. Rev. 40 (2011) 2848–2866.
[14] H. Xiong, F. Seela, J. Org. Chem. 76 (2011) 5584–5597.
[15] B.S. Holla, M. Mahalinga, M.S. Karthikeyan, B. Poojary, P.M. Akberali, N. S. Kumari, Eur. J. Med. Chem. 40 (2005) 1173–1178.
[16] M.J. Giffin, H. Heaslet, A. Brik, Y.C. Lin, G. Cauvi, C.H. Wong, D.E. McRee, J. H. Elder, C.D. Stout, B.E. Torbett, J. Med. Chem. 51 (2008) 6263–6270.
[17] H.B. Lazrek, M. Taourirte, T. Oulih, J.L. Barascut, J.L. Imbach, C. Pannecouque, M. Witrouw, E.D. Clercq, Nucleos. Nucleot. Nucleic Acids 20 (2001) 1949–1960.
[18] R. Huisgen, Angew. Chem., Int. Ed. Engl. 2 (1963) 565–598.
[19] P. Wu, V.V. Fokin, Aldrichimica Acta 40 (2007) 7–17.
[20] H.C. Kolb, M.G. Finn, K.B. Sharpless, Angew. Chem., Int. Ed. 40 (2001) 2004–2021.
[21] J. Dong, L. Krasnova, M.G. Finn, K.B. Sharpless, Angew. Chem. Int. Ed. 53 (2014) 9430–9448.
[22] C.W. Tornøe, C. Christensen, M. Meldal, J. Org. Chem. 67 (2002) 3057–3064.
[23] V.V. Rostovtsev, L.G. Green, V.V. Fokin, K.B. Sharpless, Angew. Chem., Int. Ed. 41 (2002) 2596–2599.
[24] V.D. Bock, H. Hiemstra, J.H. van Maarseveen, Eur. J. Org. Chem. (2006) 51.
[25] H.C. Kolb, K.B. Sharpless, Drug Discov. Today 8 (2003) 1128–1137.
[26] C. Spiteri, J.E. Moses, Angew. Chem. Int. Ed. 49 (2010) 31–33.

[27] W.G. Lewis, F.G. Magallon, V.V. Fokin, M.G. Finn, J. Am. Chem. Soc. 126 (2004) 9152–9153.
[28] J.E. Hein, V.V. Fokin, Chem. Soc. Rev. 39 (2010) 1302–1315.
[29] M. Meldal, C.W. Tornøe, Chem. Rev. 108 (2008) 2952–3015.
[30] R. Boobalan, C. Chen, G.-H. Lee, Catal. Commun. 107 (2018) 33–38.
[31] J. McNulty, K. Keskar, Eur. J. Org. Chem. 2012 (2012) 5462–5470.
[32] L. Zhang, X. Chen, P. Xue, H.H. Sun, I.D. Williams, K.B. Sharpless, V.V. Fokin, G. Jia, J. Am. Chem. Soc. 127 (2005) 15998–15999.
[33] E. Rasolofonjatovo, S. Theeramunkong, A. Bouriaud, S. Kolodych, M. Chaumontet, F. Taran, Org. Lett. 15 (2013) 4698–4701.
[34] X. Meng, X. Xu, T. Gao, B. Chen, Eur. J. Org. Chem. 28 (2010) 5409–5414.
[35] F.R. Gayen, A.A. Ali, D. Bora, S. Roy, S. Saha, L. Saikia, R.L. Goswamee, B. Saha, Dalton Trans. 49 (2020) 6578–6586.
[36] L. Liang, J. Ruiz, D. Astruc, Adv. Synth. Catal. 353 (2011) 3434–3450.
[37] E.F.V. Scriven, K. Turnbull, Chem. Rev. 88 (1988) 297–368.
[38] B.S.P.A. Kumar, K.H.V. Reddy, K. Karnakar, G. Satish, Y.V.D. Nageswar, Tetrahedron Lett. 56 (2015) 1968–1972.
[39] L. Cao, C. Liu, X. Tang, X. Yin, B. Zhang, Tetrahedron Lett. 55 (2014) 5033–5037.
[40] A. Akbari, N. Arsalani, M. Amini, E. Jabbari, J. Mol. Catal. A: Chem. 414 (2016) 47–54.
[41] Y. Jiang, D. Kong, J. Zhao, W. Zhang, W. Xu, W. Li, G. Xu, Tetrahedron Lett. 55 (2014) 2410–2414.
[42] B. Kaboudin, R. Mostafalu, T. Yokomatsu, Green Chem. 15 (2013) 2266–2274.
[43] C. Deraedt, N. Pinaud, D. Astruc, J. Am. Chem. Soc. 136 (2014) 12092–12098.
[44] K. Bahrami, M.S. Arabi, New J. Chem. 40 (2016) 3447–3455.
[45] P. Veerakumar, M. Velayudham, K.-L. Lu, S. Rajagopal, Catal. Sci. Technol. 1 (2011) 1512–1525.
[46] F.M. Moghaddam, S.E. Ayati, H.R. Firouzi, F. Ghorbani, Appl. Organomet. Chem. 30 (2016) 488–493.
[47] Y. Masuyama, K. Yoshikawa, N. Suzuki, K. Hara, A. Fukuoka, Tetrahedron Lett. 52 (2011) 6916–6918.
[48] M. L. Kantam, V. S. Jaya, B. Sreedhar, M. M. Rao, B. Choudary, J. Mol. Catal. 256 (2006) 273–277.
[49] H. Sharghi, R. Khalifeh, M.M. Doroodmand, Adv. Synth. Catal. 351 (2009) 207–218.
[50] Z. Zhang, C. Dong, C. Yang, D. Hu, J. Long, L. Wang, H. Li, Y. Chen, D. Kong, Adv. Synth. Catal. 352 (2010) 1600–1604.
[51] F. Alonso, Y. Moglie, G. Radivoy, M. Yus, Adv. Synth. Catal. 352 (2010) 3208–3214.
[52] N. Noshiranzadeh, M. Emami, R. Bikas, A. Kozakiewicz, New J. Chem. 41 (2017) 2658.
[53] M. Bagherzadeh, H. Mahmoudi, S. Ataie, M. Hafezi-Kahnamouei, S. Shahrokhian, G. Bellachioma, and L. Vaccaro, Inorganica Chimica Acta 492 (2019) 213–220.
[54] R. Bikas, F. Ajormal, N. Noshiranzadeh, M. Emami, A. Kozakiewicz, Appl. Organomet. Chem. 34 (2020) e5826.
[55] E. Evangelio, N.P. Rath, L.M. Mirica, Dalton Trans. 41 (2012) 8010.
[56] M. Emami, R. Bikas, N. Noshiranzadeh, A. Kozakiewicz, T. Lis, ACS Omega 5 (2020) 13344–13357.
[57] A. Banan, F. Nikbakht, S. Ataie, J. Porous Mater. 26 (2019) 1427–1433.
[58] M. Bagherzadeh, A. Bayrami, R. Kia, M. Amini, L.J.K. Cook, P.R. Raithby, Inorg. Chim. Acta 466 (2017) 398–404.
[59] R.R. Gagne, C.L. Spiro, T.J. Smith, C.A. Hamann, W.R. Thies, A.D. Shiemke, J. Am. Chem. Soc. 103 (1981) 4073–4081.
[60] Bruker, APEX2, SAINT and SADABS, BRUKER AXS, Inc. Madison, Wisconsin, USA, (2008).
[61] G.M. Sheldrick, Acta Cryst. A 64 (2008) 112–122.
[62] L.J. Farrugia, J. Appl. Cryst. 45 (2012) 849–854.
[63] G.M. Sheldrick, Acta Cryst. C 71 (2015) 3–8.
[64] A.L. Spek, Acta Cryst. D65 (2009) 148.
[65] L.J. Farrugia, J. Appl. Crystallogr. 30 (1997) 565.
[66] M. A. Spackman, D. Jayatilaka. CrystEngComm, 11 (2009) 19-32.
[67] M. A. Spackman, J. J. McKinnon. CrystEngComm, 4 (2002) 378-392.
[68] F. Neese, Wires Comput. Mol. Sci. 2 (2012) 73–78.
[69] J.P. Perdew, Phys. Rev. b: Condens. Matter Mater. Phys. 33 (1986) 8822–8824.
[70] A.D. Becke, Phys. Rev. A 38 (1988) 3098–3100.
[71] F. Neese, J. Comput. Chem. 24 (2003) 1740–1747.
[72] A. Schäfer, H. Horn, R. Ahlrichs, J. Chem. Phys. 97 (1992) 2571–2577.
[73] K. Eichkorn, O. Treutler, H. Öhm, M. Häser, R. Ahlrichs, Chem. Phys. Lett. 240 (1995) 283–290.
[74] K. Eichkorn, F. Weigend, O. Treutler, R. Ahlrichs, Theor. Chem. Acc. 97 (1997) 119–124.
[75] F. Weigend, R. Ahlrichs, Phys. Chem. Chem. Phys. 7 (2005) 3297–3305.
[76] D.A. Pantazis, X.Y. Chen, C.R. Landis, F. Neese, J. Chem. Theory Comput. 4 (2008) 908–919.
[77] S. Hirata, M. Head-Gordon, Chem. Phys. Lett. 302 (1999) 375–382.
[78] A. Klamt, G. Schüürmann, J. Chem. Soc. Perkin Trans. 2 (1993) 799–805.
[79] T. Yanai, D.P. Tew, N.C. Handy, Chem. Phys. Lett. 393 (2004) 51–57.
[80] L. Laaksonen, J. Mol. Graphics 10 (1992) 33–34.
[81] A.K. Ghosh, D. Ray, Polyhedron 52 (2013) 370–376.
[82] P. Chakraborty, J. Adhikary, B. Ghosh, R. Sanyal, S.K. Chattopadhyay, A. Bauza, A. Frontera, E. Zangrando, D. Das, Inorg. Chem. 53 (2014) 8257–8269.
[83] M. Emami, N. Noshiranzadeh, R. Bikas, A. Gutierrez, A. Kozakiewicz, Polyhedron 122 (2017) 137–146.
[84] R.J. Deeth, M.A. Hitchman, Inorg. Chem. 25 (1986) 1225–1233.
[85] J. E. Huheey, Inorganic Chemistry: Principles of Structure and Reactivity, Harper & Row, 3rd Edition (1983) 400.
[86] K.S. Banu, T. Chattopadhyay, A. Banerjee, S. Bhattacharya, E. Suresh, M. Nethaji, E. Zangrando, D. Das, Inorg. Chem. 47 (2008) 7083–7093.
[87] M. Das, G.A. Craig, D. Escudero, M. Murrie, A. Frontera, D. Ray, New J. Chem. 42 (2018) 14349–14364.
[88] L.-L. Gan, X. Li, M.-X. Du, Y.-J. Yan, Y. Zhang, W.-K. Dong, Y.-J. Ding, J. Mol. Str. 1299 (2024) 137199.
[89] L. Tong, Y.-F. Ding, X. Li, L.-L. Man, W.-K. Dong, J. Coord. Chem. 76 (2023) 1635–1649.
[90] L.-L. Gan, L. Tong, L.-L. Liu, Y.-N. Yue, W.-K. Dong, J. Mol. Struct. 1296 (2024) 136907.
[91] X. Liu, N. Novoa, C. Manzur, D. Carrillo, J. Hamon, New J. Chem. 40 (2016) 3308–3313.
[92] B. Mondal, M. Kundu, S.P. Mandal, R. Saha, U.K. Roy, A. Roychowdhury, D. Das, ACS Omega 4 (2019) 13845–13852.
[93] B.J. Sarkar, M. Kundu, B. Mondal, S. Mukherjee, A. Bandyopadhyay, U.K. Roy, J. Mol. Struct. 1274 (2023) 134493.
[94] N. Noshiranzadeh, M. Emami, R. Bikas, A. Kozakiewicz, New J. Chem. 46 (2022) 19468–19481.
[95] C.W. Tornoe, C. Christensen, M. Meldal, J. Org. Chem. 67 (2002) 3057–3064.
[96] L. Liang, D. Astruc, Coord. Chem. Rev. 255 (2011) 2933–2945.